Sustainable Energy & Fuels

Communication

Assessment of toxicity reduction in ZnS substituted CdS:P3HT bulk heterojunction solar cells fabricated using a single-source precursor deposition

Received 00th January 20 xx,
Accepted 00th January 20xx

DOI: 10.1039/x0xx00000x

www.rsc.org/

Matthew T. Bishop,[a] Marco Tomatis,[a,b] Wenjun Zhang,[c] Chuang Peng,[d,e*] George Z. Chen,[d,f] Jun He [b,d] and Di Hu [d,g*]

Utilisation of cadmium sulphide (CdS) for the preparation of hybrid bulk heterojunction (BHJ) solar cells is limited due to its high human, soil and marine toxicity. This work aims to reduce the toxicity of the cadmium based hybrid bulk heterojunctions, by varying the composition of metal sulphide nanoparticles between CdS and zinc sulphide (ZnS). Furthermore, these devices were created using a single-source precursor, which limits potential barriers for scaling up this process to industrial scale. It was found that the chemical composition of fabricated devices varied as expected; however, comparable morphologies were noted by SEM analyses. Toxicity of fabricated photovoltaic devices was estimated according to the life cycle assessment methodology, using the SimaPro software. Although negligible changes between the band gaps of prepared devices were calculated by decreasing the Cd load to 50 wt%, over 50 % reduction to human toxicity could be achieved. As a photovoltaic device, the highest power conversion efficiency (0.018 %) was observed for the device containing 75 wt% Cd and 25 wt% Zn, which also showed significant reductions for human and environmental toxicity (25 % and 19 % reduction, respectively) in comparison to the device containing only CdS, while increasing the power conversion efficiency by roughly 30 %. It was also noted that although the ZnS only device had the lowest efficiency (0.002 %, a decrease of roughly 98 %), however, this allowed for a 99 % reduction in human toxicity and a 73 % reduction in terrestrial ecotoxicity.

1. Introduction

It has been estimated that around $3x10^{24}$ J of energy reach Earth from the sun each year, which theoretically could be utilised to address the current annual world energy consumption of $8x10^{16}$ J [1, 2]. Establishing effective methods of harvesting solar energy could potentially reduce the utilisation of fossil fuels for power generation and therefore, be a great benefit to society. Over 85 % of commercially available solar cells are silicon based [3]. However, the production of 1 Mt of silicon has been shown to release roughly 1.58 Mt of CO2 into the atmosphere [4]. This poses a significant, and often overlooked, impact on the environment.

Bulk heterojunction (BHJ) solar cells provide a potential alternative method of harvesting solar energy. BHJs refer to multiple phases mixed within one layer. The heterojunction provides a three-dimensional blend of electron-donating and electron-accepting materials characterised by a large donor/acceptor interface area which increases the probability of exciton capture and dissociation, thereby increasing the potential power output of the solar cells [5-7]. Furthermore, it has been suggested that creating BHJs composing of both conductive organic polymers and inorganic nanocrystals could combine material advantages, such as flexibility and stability, of organic and inorganic devices [8]. However, the synthesis of these devices often requires multiple steps, causing complications for large scale implementation for future commercialisation opportunities [1, 5, 6, 9].

With regard to the fabrication of BHJs for energy harvesting applications, poly(3-hexylthiophene) (P3HT) is commonly used as the organic component, due to its high absorption coefficient (roughly 10^5 cm^{-1}) within the visible region of the solar spectrum [3, 8]. Whereas for the inorganic component, metal sulphides have been extensively studied [10, 11]. A novel single source precursor mixture was used in order to deposit a metal sulphide/polymer matrix in a more efficient and easier scale-up method, as a means to overcome the often complicated synthetic route for BHJs. This requires a precursor with an appropriately low decomposition temperature precursor for

[a] International Doctoral Innovation Centre, University of Nottingham Ningbo China, Ningbo, 315100, PR China
[b] Research Group of Natural Resources and Environment, Faculty of Science and Engineering, University of Nottingham Ningbo China, 315100, PR China
[c] Ningbo Institute of Materials Technology and Engineering, Chinese Academy of Sciences, Ningbo 315201, China
[d] Department of Chemical and Environmental Engineering, Faculty of Science and Engineering, University of Nottingham Ningbo China, 315100, PR China
[e] Wuhan University, School of Resource and Environmental Science, Wuhan 30079, Hubei, PR China
[f] Department of Chemical and Environmental Engineering, Advanced Materials Research Group, Faculty of Engineering, University of Nottingham, Nottingham NG7 2RD, UK
[g] Advanced Energy and Environmental Materials & Technologies Research Group, The University of Nottingham Ningbo China, Ningbo 315100, PR China
*– Chuang.peng@whu.edu.cn and Di.Hu@nottingham.edu.cn

the synthesis of the metal sulphide nanoparticles, as polymers are usually thermally unstable [12, 13].

Cadmium sulphide (CdS) has been a proven inorganic component for the abovementioned applications [14-18], however, it is a highly toxic material rendering a high impact to both the human health and the environment. Therefore, it is paramount to design a hybrid photovoltaic device of comparable or higher efficiency to the more conventional CdS based ones by utilising non-toxic or less toxic compounds. ZnS has emerged as a potential substitute for CdS due to its relatively low toxicity and high open circuit voltage [19]. However, its application as a substitute for CdS in photovoltaic devices has been scarcely investigated, especially using the comparable deposition procedures to allow for accurate comparative studies [15, 19, 20].

In order to address this research gap, the efficiencies of photovoltaic devices prepared at varying weight ratios of CdS and ZnS have been investigated. Photovoltaic devices described in this study were prepared via decomposition of metal ethyl xanthate precursors (MXan, M= Cd, Zn), at varying metal concentrations, dispersed within a P3HT matrix using spin coating deposition. MXan were selected as precursors due to their low decomposition temperature, which allows preventing damage to the polymeric component, and have been previously shown to form functional BHJ photovoltaic devices [9, 21]. MXan have been thought to decompose to metal sulphides via the Chugaev elimination reaction [22], a reaction mechanism consisting of a syn-elimination of an alkene via a 6-membered cyclic transition state, carbonyl sulphide elimination and a hydrogen sulphide elimination process (**Figure 1**).

Relationships between the chemical composition and properties of prepared hybrid BHJ photovoltaic device were then established to investigate whether ZnS could be used as an alternative to partly, or completely replace CdS in hybrid BHJ solar cells. In addition, the toxicity related to the disposal of produced solar cells as landfill waste was quantified according to the principle of the Life Cycle Assessment (LCA), a widely applied methodology which allows assessing the environmental impact of processes and products throughout their whole life cycle [23].

2. Experimental

2.1. Toxicity Assessment

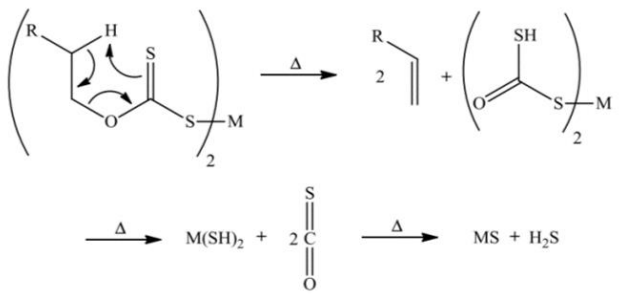

Figure 1. The general reaction mechanism for Chugaev elimination reaction.

As the fabrication of BHJ solar cells is currently only at laboratory scale [12, 14], it was not possible to assess the potential environmental impact of prepared photovoltaic devices during their whole life cycle. It is also worth highlighting that laboratory scale processes are sub-optimal, as they do not consider precursor recycling or other strategies aimed at minimising the amount of reagents used and wastes produced. Therefore, results of the impact assessment describing the proposed synthetic route would not be representative of a proper production process and thus, they should not be considered. Due to this reason, only the toxicity related to the disposal of prepared devices in landfill was considered for this study. Landfill disposal was analysed as it is a common method of deposal for many items; including solar panels. Solar panels are rarely recycled due to the complexity of their structure which includes metals, plastics and various polymers, resulting in the leaching of toxic compounds and subsequent contamination of both soil and groundwater sources are commonly observed in landfill sites [24, 25]. Furthermore, by conducting this analysis at the end of the life cycle, any efforts to encapsulate and prevent metal contamination of the devices is likely to be undone due to breakages occurring, which would result in the leaching of BHJ materials.

This assessment allowed for the quantification of the changes in the toxicity of disposed solar cells towards humans and the environment based on the changes in their metal composition. Therefore, such a preliminary study could be used to complement data regarding the performance of prepared devices, aiding with the selection of different, less hazardous, precursors; possibly leading to the development of more sustainable technologies for renewable energy generation.

The impact assessment was conducted, by utilising the SimaPro software version 8.3, according to the ReCiPe method at midpoint level based on the hierarchist perspective [26]. The ReCiPe method was chosen for this study because of the relevance of the impact categories considered, including Human Toxicity (HT), Terrestrial Ecotoxicity (TET), Freshwater Ecotoxicity (FET) and Marine Ecotoxicity (MET), which allowed for the quantification of the toxicity of prepared solar cells on both humans and the environment. The metals and their concentrations utilised for the toxicity assessment were based on the discussed synthetic routes described in the following section (2.3 Device Fabrication).

It is worth mentioning here that the concentration of contaminants in landfills leachate depends on several factors including climatic conditions, waste composition, age and degradation of the considered waste [25]. Therefore, high uncertainties are expected regarding the metals concentration in soil and water since a case-by-case evaluation, based on on-site analysis, would be necessary to measure their concentration and distribution in the local environment.

2.2. Xanthate Synthesis

Each xanthate precursor was synthesised via an adapted synthetic procedure proposed by Agrawal el al [12], using either 1 g of cadmium chloride or 0.7 g of zinc chloride dissolved in 20

ml of de-ionized water. This was added to an aqueous solution containing 3.5 g of potassium ethyl xanthate dissolved in 20 ml of de-ionized water, and then stirred for 24 hours revealing a pale yellow Cadmium Xanthate (CdXan) or white Zinc Xanthate (ZnXan) precipitate. Finally, the prepared precipitate was filtered, washed with de-ionized water and dried at 50 °C.

2.3. Device fabrication

Prior to deposition, substrates were ultra-sonically cleaned in ethanol for 10 minutes and dried in an inert gas.
Five precursors were prepared at different metal compositions:

- 0.442 g of CdXan and 0 g of ZnXan (Cd4:Zn0)
- 0.332 g of CdXan and 0.142 g of ZnXan (Cd3:Zn1)
- 0.221 g of CdXan and 0.284 g of ZnXan (Cd2:Zn2)
- 0.111 g of CdXan and 0.426 g of ZnXan (Cd1:Zn3)
- 0 g of CdXan and 0.568 g of ZnXan (Cd0:Zn4)

Each precursor was dissolved in 10 ml of 1,2-dichlorobenzene (DCB) with 0.18 g of P3HT. The prepared solutions were then pipetted onto indium tin oxide (ITO) coated glass and spin coated at 1000 rpm for 30 seconds. These deposition parameters were chosen as the optimised condition for Cd4:Zn0 and result in a film roughly 70-80 nm thick (**Figure 2**). After the deposition, devices were heated to 160 °C for 30 minutes, to decompose the xanthate precursors into their respective sulphides.
Once the active layers have been deposited, an additional 50 nm layer of gold was coated to the device via DC-magnetron sputtering, to work as an electrode for the device. Gold was selected as it is a highly conductive and non-toxic material that has been previously used for photovoltaic applications [27]. A current of 11 mA was utilised for this deposition, as it was noted that higher currents caused the device to fail. This is likely due to penetration between layers, resulting in the destruction of the architecture of the BHJ. A schematic of the final device design is shown in **Figure 3** and photographs of deposited samples are shown in **Figure 4**. From **Figure 4** it can be seen that deposition occurs successfully, without any damage to the surface of the decomposed film.

2.4. Characterisation techniques

To determine the crystal structure, X-ray diffraction (XRD) patterns were collected using a D8 Advance diffractometer (Bruker) equipped with a copper anode (Cu-Kα radiation λ = 0.154 nm) over the angular range of $10^{o} < 2\theta < 90^{o}$ with a step size of 0.01^{o} at 40 kV and 35 mA.
A Zeiss ΣIGMA Scanning Electron Microscopy (SEM) operating at 5.0 kV was used for knowing the morphology, size of the deposited films, while the composition was analysed by Energy Dispersive Spectroscopy (EDS) on an X-Act (Oxford Instrument) coupled with the previously mentioned SEM.
Thicknesses of deposited layers were determined using a Veeco 3100 SPM in tapping mode to collect line profiles of these layers.
Optical characteristics of the samples were measured at room temperature using a Cary 5000 UV-vis absorption spectrometer at a rate of 400 nm/s, between 350 – 750 nm. One cycle was taken for each sample.

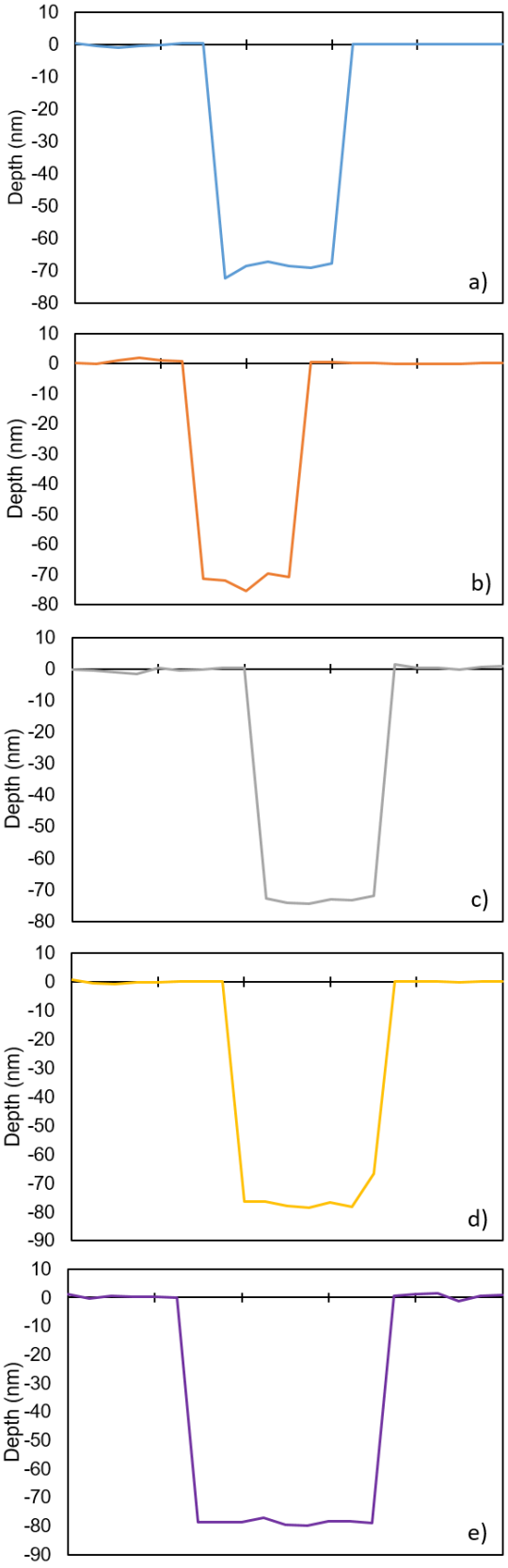

Figure 2. AFM line profiles to determine the thickness of a) Cd4:Zn0, b) Cd3:Zn1, c) Cd2:Zn2, d) Cd1:Zn3 and e) Cd0:Zn4.

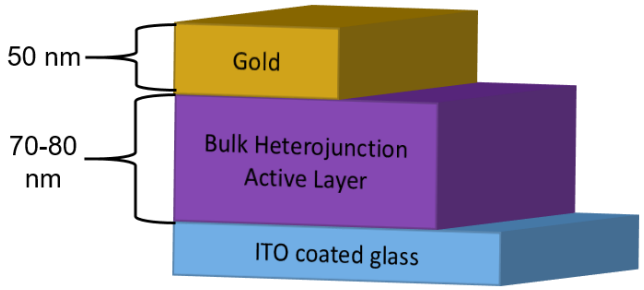

Figure 3. Schematic representation of the device design.

Current-voltage measurements were made using a CHI600E electrochemical workstation under illumination at AM1.5 G (100 mW cm^{-2}) light intensity.

3. Results and Discussion

3.1. Toxicity Assessment

Figure 5 represents the toxicity assessment for the disposal of prepared BHJ solar cells in landfill. It is worth mentioning LCA describing the production and utilisation of solar panels in photovoltaic plants or on a domestic scale rarely considered the end of life of the panels due to the lack of data describing this stage [28]. However, the behaviour of heavy metals leachates as well as possible remediation strategies are widely described, allowing to justify toxicities distributions reported in **Figure 5** [29, 30]. The severe toxicity of heavy metal leachates is mainly related to the contamination of soil, surface and groundwater. These contaminations lead to the bioaccumulation of toxic metals in various organisms and therefore cause significant impacts to both human health and the environment [31].

As expected, reduction of the toxicity ranging between 99% and 19% for human toxicity and freshwater ecotoxicity, respectively

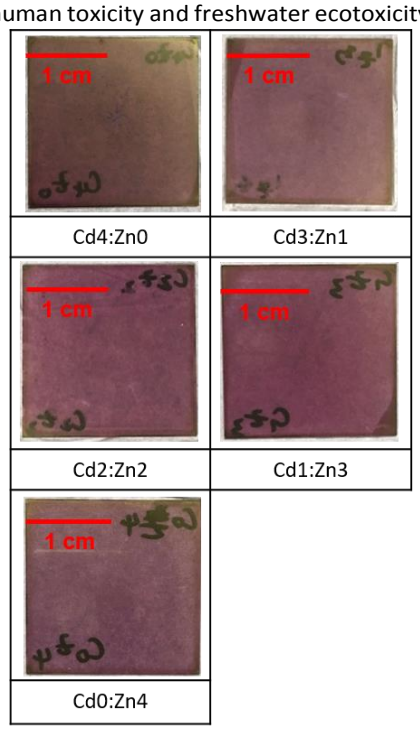

Figure 4. Photographs taken of deposited and decomposed samples, prior to gold deposition.

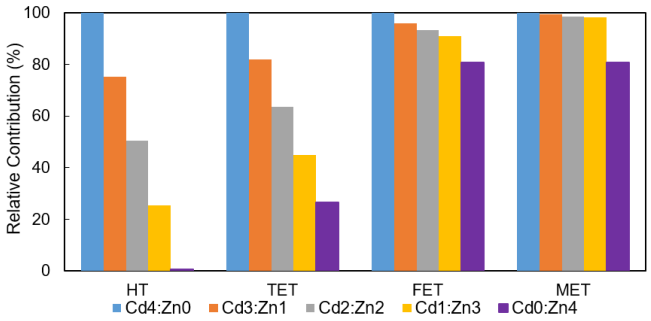

Figure 5. Relative contribution to human and environmental toxicity of prepared samples. Showing Human Toxicity (HT), Terrestrial Ecotoxicity (TET), Freshwater Ecotoxicity (FET) and Marine Ecotoxicity (MET).

were observed with the decrease of CdS load. The toxicity of devices prepared at higher CdS loads was mainly attributed to the widely described toxicity of Cd to several organs [32], to soil [33] and water [34]. It is worth highlighting that only moderate reductions of the toxicity of prepared devices were observed on fresh and marine water (up to 19% reduction on FET and MET). This was possibly because Zn was proven toxic towards various aquatic organisms at different stages of their life [35]. On the contrary, the toxicity of Zn towards humans and soils resulted in dramatic reductions. The scarce toxicity of this metal was attributed to the fact that Zn is utilised by the human body and it becomes toxic only at high concentrations [36], while its toxicity in soils mostly depends on the type and properties of considered soil [37]. Therefore, dramatic reductions of the environmental impact were observed with the increase of ZnS metal load on human toxicity and terrestrial ecotoxicity (up to 99 % and 73% reduction were estimated for Cd0:Zn4 on HT and TET, respectively).

3.2. Characterisation of Cd-Zn based solar cells

XRD (**Figure 6**) and SEM coupled with EDS (**Figure 7)** analyses were utilised as preliminary tests in order to determining the composition and to quantify the altering chemical composition of the deposited layer.

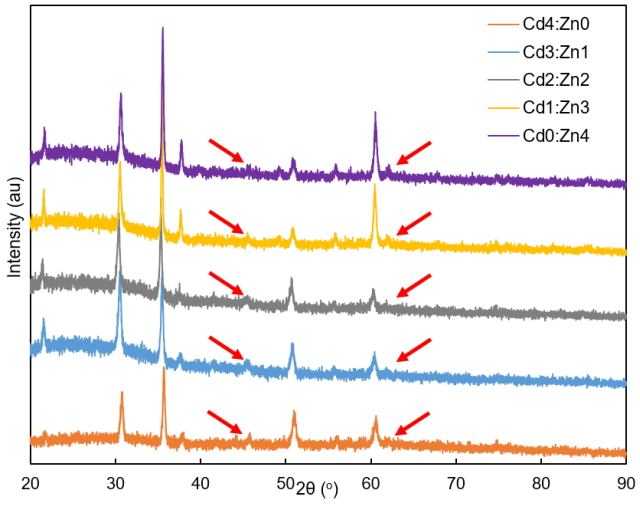

Figure 6. XRD analysis of films, deposited on ITO coated glass. Key peaks at 48 and 63 ° (2Θ), for CdS and ZnS respectively, are highlighted by red arrows.

Figure 6 shows the XRD diffractograms of the deposited active layers as the ratio of the precursors change. Characteristic ITO peaks [38], from the substrate, (JCPDS No. 71-2194) could be seen at roughly 2θ=30, 36, 38, 51, 61 °. Typical diffraction peaks of CdS Greenockite [39] (JCPDS No. 41-1049) were observed at around 25, 26, 28, 44, 48, 52 and 61 ° (2θ), while diffraction peaks located at 27, 28, 30, 40, 56 and 63° (2θ) suggested the presence of ZnS Wurtzite [40] (JCPDS No. 79-2204) on analysed samples. The diffraction peaks of CdS, ZnS and ITO often align; however, two noticeable peaks, located at roughly 48 and 63 ° (2θ) for CdS and ZnS respectively. To highlight these peaks, red arrows are used in **Figure 6**.

As expected, the intensity of diffraction peaks of CdS gradually decreased with the increase of ZnS load and were not be observed during the analysis of Cd0:Zn4. The smaller shoulder peak at 63 °, corresponding to ZnS, decreases in intensity with decreasing ZnS load in the device.

From **Figure 7** it is apparent that all samples have a similar morphology, regardless of their chemical composition. This suggests that the substrate or P3HT are the predominant factors in the determination of the morphology. EDS analysis results reported in **Figure 7** also confirmed the variation of the metal content suggested by the XRD results showing atomic ratios comparable to those expected from the deposition conditions, confirming varying metal ratios required for this study.

UV-vis analysis of deposited films was also conducted, as reported in **Figure 8**.

Each absorption spectra displays a small peak at roughly 605 nm, which was attributed to the ordering of intra-chain interactions in P3HT [12]. Deposited films with higher concentrations of CdS such as Cd4:Zn0 and Cd3:Zn1, present an initial peak position that is noticeably more red-shifted compared to their ZnS counterparts. This pushes their peak absorption to overlap more significantly with the solar spectrum, which peaks at roughly 530 nm. Comparable red-shifts where also reported by Jabeen *et al* [41] during their investigation of Cd doped ZnS nanoparticles. According to the authors, such shift would enable the band gap to be tuned for more absorption in the visible spectra.

In order to better understand the optical properties of the active layers, Tauc plots were generated form the spectral data, plotting $(\alpha h\nu)^2$ vs hν (see **Figure 9**). From these plots, the band gaps can be estimated by extrapolating the straight line of the Tauc plot to intercept the X-axis [42].

These generated Tauc plots were used to calculate the band gap energies of the devices, to properly investigate this effect the chemical composition has on band gap tuning (**Figure 9**) [13, 43, 44]. The main peak in the solar spectrum occurs at roughly 530 nm, which corresponds to a band gap of 2.33 eV.

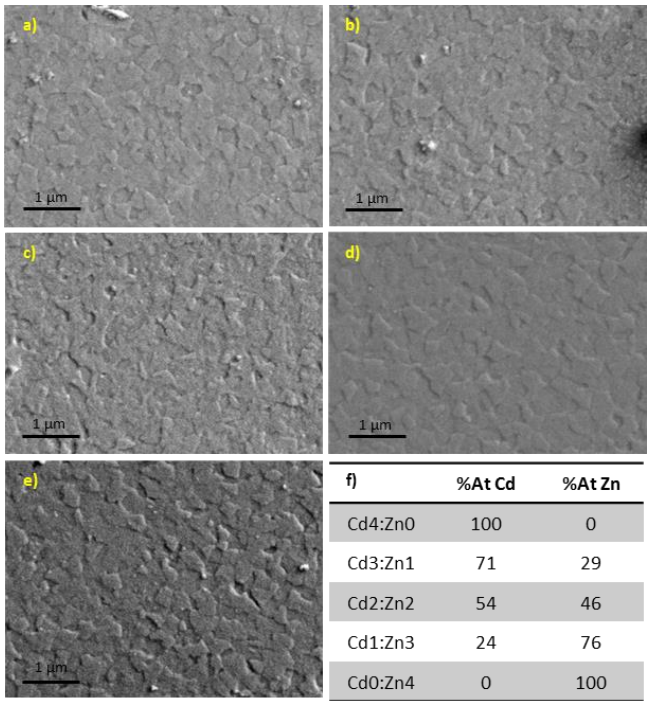

f)	%At Cd	%At Zn
Cd4:Zn0	100	0
Cd3:Zn1	71	29
Cd2:Zn2	54	46
Cd1:Zn3	24	76
Cd0:Zn4	0	100

Figure 7. SEM images of a) Cd4:Zn0, b) Cd3:Zn1, c) Cd2:Zn2, d) Cd1:Zn3, e) Cd0:Zn4 and f) a table presenting the calculated atomic ratios using the EDS.

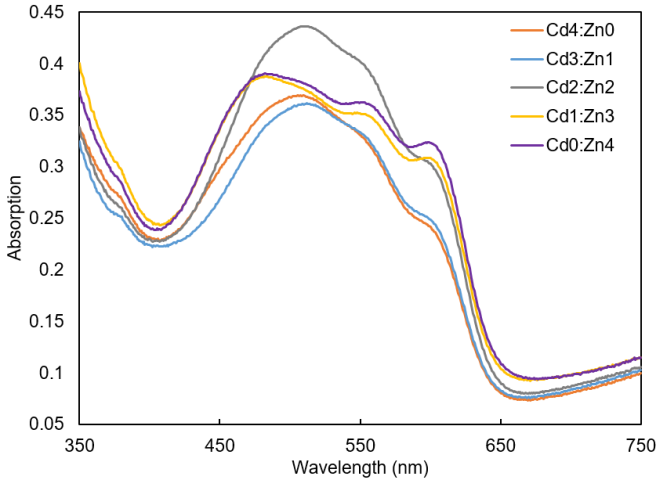

Figure 8. UV-vis analysis of films, deposited on ITO coated glass.

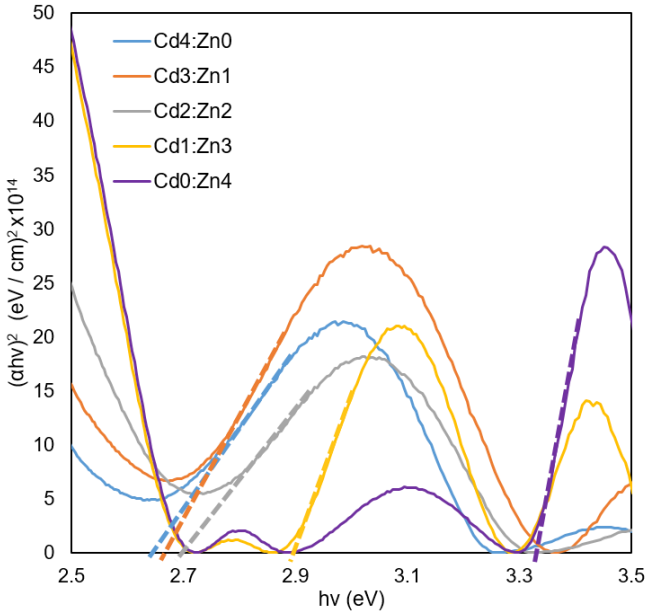

Figure 9. Tauc plots of deposited films on ITO coated glass.

However, it has been reported that peak efficiencies for single-junction devices, like the devices described in this work, occur with a band gap between 1.3-1.75 eV [45, 46]. It was calculated that the band gap for the Cd4:Cd0 sample is 2.62 eV, and only increases by 0.05 eV with a 50 % reduction of CdS load. This band gap then increases to 2.89 eV as the concentration of Zn surpasses that of Cd (Cd1:Zn3), and finally is noted to be 3.33 eV for Cd0:Zn4. From the results shown in **Table 1** it can be inferred that the observed band is proportional to the concentration of Cd and inversely proportional to the concentration of Zn. This increase in band gap can only be attributed to the content of ZnS as no other changes in deposition took place and the morphology of the material remains constant.

As reported in **Table 1**, the band gap of Cd4:Zn0 was closer to the optimum values (1.3-1.75 eV) in comparison to that estimated for pure ZnS (Cd0:Zn4). This is due to the red-shifting observed with increasing CdS content, allowing for better overlap with the solar spectrum. However, since the observed band gap increased by 0.05 eV from Cd4:Zn0 to Cd2:Zn2, it has been shown that the CdS content can be reduced with minimal effect to the calculated band gap. Though, it is important to note that the band gap is not the sole factor that alters the performance of a photovoltaic device.

The current-voltage (I–V) plots of prepared samples were also measured to determine the influence of the abovementioned chemical and optical differences on key photovoltaic parameters, see **Figure 10**. It is important to note that there is non-linear relationship between the chemical characteristics of the devices and their respective photovoltaic parameters. This is reflected in the relative positions of the curves displayed in **Figure 10**, showing that the reduction of CdS to a 75% load (Cd3:Zn1) outperformed the pure CdS sample (Cd4:Zn0). This could partially be due to the doping effects, such as the potential increase in the energy of conduction band of the inorganic phase, promoting charge diffusion, and the stability of the band gap of the material [41, 47]. The efficiency was considerably decreased with further increase in Zn load, despite the continued stability of the band gap. The formation of an additional phase of ZnS would hinder charge transport within the material, by increasing path length [41]. Therefore it is hypothesised to be the cause of these findings and result in a lower efficiency device.

Table 2 displays the average characteristic photovoltaic parameters for 3 replicates of each device tested. The maximum voltage available from the photovoltaic devices, open-circuit voltage (Voc), for Cd4:Zn0 and Cd0:Zn4 are consistent with values previously reported for CdS:P3HT [16], and ZnS:P3HT [20]

Sample name	Band gap (eV)	Percentage Variation from Cd4:Zn0
Cd4:Zn0	2.62	-
Cd3:Zn1	2.65	+1.1 %
Cd2:Zn2	2.67	+2.0 %
Cd1:Zn3	2.89	+10.3 %
Cd0:Zn4	3.33	+27.1 %

Table 1. Optical band gaps of active layers of different compositions.

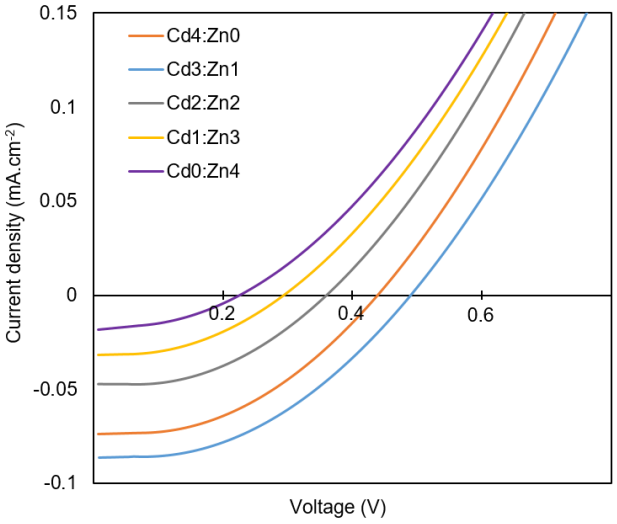

Figure 10. I-V plots of CdS/ZnS:P3HT devices under illumination with an intensity of 100 mW.cm^{-2}.

photovoltaic devices. Initial introduction of Zn into the device, Cd3:Zn1, has an enhanced Voc, increasing it from 0.44 to 0.49 V. This is likely due to the increase in band gap, as it has been shown that the band gap and Voc are directly related therefore, increases in the band gap lead to increases in the Voc [45, 48]. Furthermore, it is important to note that the varying Voc, with altering precursor chemical compositions, demonstrates the formation of CdS-ZnS heterojunctions. Since the Voc are determined by the energy gaps between the donor and acceptor materials, the variation in this value displays the chemical and electrical alteration of these layers and therefore the energy levels of the system [49,50].

The trend seen in Voc is mimicked in the collected short-circuit current (Jsc) values, with Cd3:Zn1 showing the highest value (0.084 mA.cm^{-2}) and Cd0:Zn4 showing the lowest value (0.015 mA.cm^{-2}). This analysis clearly showed that ZnS based solar cells collect lower currents than their CdS counterparts. It is important to note that Jsc values reported in **Table 2** are also influenced by resistance between different components of the device. This can be dramatically improved through various methods, such as energy level optimisation via introducing layers to enhance carrier mobility and current collection or

	Voc (V)	Jsc (mA.cm^{-2})	Fill Factor	PCE (%)
Cd4:Zn0	0.44	0.072	0.45	0.014
Cd3:Zn1	0.49	0.084	0.45	0.018
Cd2:Zn2	0.36	0.046	0.46	0.008
Cd1:Zn3	0.30	0.031	0.45	0.004
Cd0:Zn4	0.23	0.015	0.47	0.002

Table 2. Average characteristic photovoltaic parameters of devices derived from current-voltage plots

altering the chemistry of current layers through the introduction of additional dopants [7, 20, 51].

The Fill Factor (FF) is the ratio of the maximum power of the device to the product of the Voc and Jsc. As shown in **Table 2**, the FF for the different devices remained fairly constant. This would suggest a similar recombination mechanism and quenching for each device, which is likely as the shown morphology (**Figure 5**) appears to be the same regardless of the sample. Since recombination often occurs at grain boundaries, the FF is likely to vary as the morphology varies [10]. The Power Conversion Efficiencies (PCEs) reported in **Table 2** follow the same trend observed for both Voc and Jsc, due to the correlation of these three parameters with the efficiency.

From the PCEs it can be said that the Cd3:Zn1 device performs the best. This can be attributed to two major factors, the increase in Voc and the increase in Jsc. As previously discussed, the increased Voc is due to the manipulation of energy levels from the incorporation of ZnS in the device. The increased Jsc value could potentially be attributed to two things, either the optical properties or collection properties of the device [52]. As the absorption is lower (**Figure 8**) and the band gap (**Figure 9**) is less favourable than that for Cd4:Zn0. Therefore, the enhancement can be attributed to collection properties. The incorporation of ZnS into a CdS acceptor material has been suggested to improve collection properties by improving the transportation of electrons into the acceptor phase [53].

4. Conclusions

This investigation looked into the potential reduction of CdS used in newly deposited BHJ photovoltaics, to help increase the possible future commercial viability of these devices. Five variations of CdS/ZnS:P3HT BHJs were deposited and characterised from single source precursors. It was shown that by using higher concentrations of CdXan in the precursor solution the band gaps calculated are significantly more red-shifted. However, the band gap only changes by 2 % with a 50 % reduction of CdS in the device, which roughly equates to a 50 % reduction in human toxicity. Overall, Cd3:Zn1 resulted the most efficient solar device prepared in this study, showing the reduction of CdS load used in the device. This results in a toxicity reduction of up to 25% for human toxicity and 19% for the environment. However, all devices were shown to be functional, that a single-source precursor could be used to create any of these devices for ease of commercialisation. While the higher Zn loaded devices performed worse compared to their more toxic counterparts. With further development of the potential for these efficiencies to be improved is very possible, which could help to replace Si solar cells with low toxicity single-source precursor solar cells. This work demonstrates the feasibility of using ZnS:P3HT to fabricate BHJ solar cells, and the potential of reducing the toxicity of CdS:P3HT based BHJ solar cells, by partly replacing CdXan in the single source precursor solution with ZnXan. These findings have provided a new pathway to develop BHJ photovoltaic devices with comparable efficiency and reduced toxicity.

Conflicts of interest

There are no conflicts to declare.

Acknowledgements

This work is supported by the International Doctoral Innovation Centre, Ningbo Education Bureau, Ningbo Science and Technology Bureau, and the University of Nottingham; Natural Science Foundation of China with a project code 51804172; the Engineering and Physical Sciences Research Council (grant number EP/J000582/1, EP/F026412/1, EP/G037345/1, EP/L016362/1); Ningbo Municipal Government (3315 Plan, 2014A35001-1, International Cooperation Plan 201501CX-C01006).

References

1. B. Parida, S. Iniyan and R. Goic, *Renewable & Sustainable Energy Reviews*, 2011, **15**, 1625-1636.
2. W. B. O. Data, Electric power consumption (kWh per capita), 2018).
3. S. Sharma, Natasha and A. Kapoor, *Journal of Renewable and Sustainable Energy*, 2014, **6**, 1-12.
4. C. Breitkopf and K. Swider-Lyons, *Springer Handbook of Electrochemical Energy*, Springer, 2016.
5. A. Nozik, *Nanostructured and Photochemical Systems for Solar Photon Conversion*, Imperial College Press, 2008.
6. B. J. Moon, G. Y. Lee, M. J. Im, S. Song and T. Park, *Nanoscale*, 2014, **6**, 2440-2446.
7. R. Kroon, M. Lenes, J. C. Hummelen, P. W. M. Blom and B. De Boer, *Polymer Reviews*, 2008, **48**, 531-582.
8. W. Jaimes, G. Alvarado-Tenorio, C. Martinez-Alonso, A. Quevedo-Lopez, H. L. Hu and M. E. Nicho, *Materials Science in Semiconductor Processing*, 2015, **37**, 259-265.
9. M. Bishop, B. Akinwolemiwa, L. Zhang, C. Peng and D. Hu, *E3S Web of Conferences*, 2019, **80**, 03012.
10. S. Aslam, F. Mustafa, M. A. Ahmad, M. Saleem, M. Idrees and A. S. Bhatti, *Ceramics International*, 2018, **44**, 402-408.
11. K. L. Chopra, P. D. Paulson and V. Dutta, *Progress in Photovoltaics*, 2004, **12**, 69-92.
12. V. Agrawal, K. Jain, L. Arora and S. Chand, *Journal of Nanoparticle Research*, 2013, **15**, 1-14.
13. M. A. Buckingham, A. L. Catherall, M. S. Hill, A. L. Johnson and J. D. Parish, *Crystal Growth & Design*, 2017, **17**, 907-912.
14. U. B. Cappel, S. A. Dowland, L. X. Reynolds, S. Dimitrov and S. A. Haque, *Journal of Physical Chemistry Letters*, 2013, **4**, 4253-4257.
15. B. Singh and A. Kaur, *Synthetic Metals*, 2014, **195**, 306-311.
16. N. Kumar and V. Dutta, *Journal of Colloid and Interface Science*, 2014, **434**, 181-187.
17. U. Jabeen, T. Adhikari, D. Pathak, S. M. Shah and J. M. Nunzi, *Optical Materials*, 2018, **78**, 132-141.
18. R. K. Bhardwaj, H. S. Kushwaha, J. Gaur, T. Upreti, V. Bharti, V. Gupta, N. Chaudhary, G. D. Sharma, K. Banerjee and S. Chand, *Materials Letters*, 2012, **89**, 195-197.
19. M. Bredol, K. Matras, A. Szatkowski, J. Sanetra and A. Prodi-Schwab, *Solar Energy Materials and Solar Cells*, 2009, **93**, 662-666.

20. U. Jabeen, T. Adhikari, S. M. Shah, D. Pathak, T. Wagner and J. M. Nunzi, *European Physical Journal-Applied Physics*, 2017, **78**, 34809.
21. P. S. Nair, T. Radhakrishnan, N. Revaprasadu, G. Kolawole and P. O'Brien, *Journal of Materials Chemistry*, 2002, **12**, 2722-2725.
22. M. Al-Shakban, P. D. Matthews and P. O'Brien, *Chemical Communications*, 2017, **53**, 10058-10061.
23. I. O. f. Standardization, *Environmental Management - Life Cycle Assessment - Principles and Framework*, 2006, **ISO 14040:2006**.
24. F. Cherubini, S. Bargigli and S. Ulgiati, *Energy*, 2009, **34**, 2116-2123.
25. A. Stefanakis, C. S. Akratos and V. A. Tsihrintzis, *Vertical Flow Constructed Wetlands*, Elsevier, Boston, 2014, pp. 145-164.
26. M. Goedkoop, M. Huijbregts, A. D. Schryver, J. Struijs and R. v. Zelm, *ReCiPe 2008: A Life Cycle Impact Assessment Method which Comprises Harmonized Category Indicators at the Midpoint and The Endpoint Level. Report I: Characterisation*, Netherlands, 2013.
27. J. Tang, K. W. Kemp, S. Hoogland, K. S. Jeong, H. Liu, L. Levina, M. Furukawa, X. H. Wang, R. Debnath, D. K. Cha, K. W. Chou, A. Fischer, A. Amassian, J. B. Asbury and E. H. Sargent, *Nature Materials*, 2011, **10**, 765-771.
28. C. E. L. Latunussa, F. Ardente, G. A. Blengini and L. Mancini, *Solar Energy Materials and Solar Cells*, 2016, **156**, 101-111.
29. M. D. Vaverkova, D. Adamcova, M. Radziemska, S. Voberkova, Z. Mazur and J. Zloch, *Waste and Biomass Valorization*, 2018, **9**, 503-511.
30. S. A. Al Raisi, H. Sulaiman, F. E. Suliman and O. Abdallah, *International Journal of Environmental Science and Development*, 2014, **5**, 60.
31. C. M. Chen and M. C. Liu, *Science of the Total Environment*, 2006, **359**, 120-129.
32. J. Godt, F. Scheidig, C. Grosse-Siestrup, V. Esche, P. Brandenburg, A. Reich and D. A. Groneberg, *Journal of Occupational Medicine and Toxicology*, 2006, **1**, 22.
33. J. L. Moreno, T. Hernandez, A. Perez and C. Garcia, *Applied Soil Ecology*, 2002, **21**, 149-158.
34. M. A. Rzetala, *Journal of Soils and Sediments*, 2016, **16**, 2458-2470.
35. J. Besser and K. Leib, *Aquatic Toxicology*, 2007, **84**, 236–246.
36. W. H. Organization, *Zinc in Drinking-water*, Geneva, 1996.
37. E. Smolders, J. Buekers, I. Oliver and M. J. McLaughlin, *Environmental Toxicology and Chemistry*, 2004, **23**, 2633-2640.
38. A. Salehi, *Thin Solid Films*, 1998, **324**, 214-218.
39. M. A. Ehsan, H. N. Ming, M. Misran, Z. Arifin, E. R. T. Tiekink, A. P. Safwan, M. Ebadi, W. J. Basirun and M. Mazhar, *Chemical Vapor Deposition*, 2012, **18**, 191-200.
40. Z. X. Deng, C. Wang, X. M. Sun and Y. D. Li, *Inorganic Chemistry*, 2002, **41**, 869-873.
41. U. Jabeen, S. M. Shah, N. Hussain, A. Fakhr e, A. Ali, A. Khan and S. U. Khan, *Journal of Photochemistry and Photobiology a-Chemistry*, 2016, **325**, 29-38.
42. M. Sampath, K. Sankarasubramanian, J. Archana, Y. Hayakawa, K. Ramamurthi and K. Sethuraman, *Materials Science in Semiconductor Processing*, 2018, **87**, 54-64.
43. A. B. Murphy, *Solar Energy Materials and Solar Cells*, 2007, **91**, 1326-1337.
44. R. O. Yathisha and Y. A. Nayaka, *Journal of Materials Science*, 2018, **53**, 678-691.
45. O. D. Miller, E. Yablonovitch and S. R. Kurtz, *Ieee Journal of Photovoltaics*, 2012, **2**, 303-311.
46. S. Rühle, *Solar Energy*, 2016, **130**, 139-147.
47. T. P. Nguyen, T. T. Ha, T. T. Nguyen, N. P. Ho, T. D. Huynh and Q. V. Lam, *Electrochimica Acta*, 2018, **282**, 16-23.
48. A. Belfar, B. Amiri and H. Ait-kaci, *Journal of Nano- and Electronic Physics*, 2015, **7**, 7.
49. H. P. Zhou, W. C. Hsu, H. S. Duan, B. Bob, W. B. Yang, T. B. Song, C. J. Hsu and Y. Yang, *Energy & Environmental Science*, 2013, **6**, 2822-2838.
50. J. Kim, G. Kim, T. K. Kim, S. Kwon, H. Back, J. Lee, S. H. Lee, H. Kang and K. Lee, *Journal of Materials Chemistry A*, 2014, **2**, 17291-17296.
51. Y. S. Kwon, J. Lim, H. J. Yun, Y. H. Kim and T. Park, *Energy & Environmental Science*, 2014, **7**, 1454-1460.
52. M. Wright and A. Uddin, *Solar Energy Materials and Solar Cells*, 2012, **107**, 87-111.
53. K. W. Sun, J. L. Huang, C. Yan, A. B. Pu, F. Y. Liu, H. Sun, X. Liu, Z. Fang, J. A. Stride, M. Green and X. J. Hao, *Chemistry of Materials*, 2018, **30**, 4008-4016.

